Analyzing the effect of slotted foil on radiation pulse profile in a mode locked afterburner X-ray free electron laser

Sandeep Kumar, Min Sup Hur, and Moses Chung

Citation: Journal of Applied Physics **121**, 243101 (2017); doi: 10.1063/1.4984936
View online: http://dx.doi.org/10.1063/1.4984936
View Table of Contents: http://aip.scitation.org/toc/jap/121/24
Published by the American Institute of Physics

Analyzing the effect of slotted foil on radiation pulse profile in a mode locked afterburner X-ray free electron laser

Sandeep Kumar, Min Sup Hur,[a] and Moses Chung[a]
Department of Physics, Ulsan National Institute of Science and Technology (UNIST), Ulsan 44919, South Korea

(Received 27 March 2017; accepted 22 May 2017; published online 22 June 2017)

Extremely short X-ray pulses in the attosecond (as) range are important tools for ultrafast dynamics, high resolution microscopy, and nuclear dynamics study. In this paper, we numerically examine the generation of gigawatt (GW) mode-locked (ML) multichromatic X-rays using the parameters of the Pohang Accelerator Laboratory (PAL)-X-ray free electron laser (XFEL), the Korean XFEL. In this vein, we analyze the ML-FEL [Thompson and McNeil, Phys. Rev. Lett. **100**, 203901 (2008)] and mode-locked afterburner (MLAB) FEL [Dunning *et al.*, Phys. Rev. Lett. **110**, 104801 (2013)] schemes on the hard X-ray beamline of the PAL-XFEL. Using the ML scheme, we numerically demonstrate a train of radiation pulses in the hard X-ray (photon energy ~12.4 keV) with 3.5 GW power and 16 as full-width half maximum (FWHM) pulse duration. On the other hand, using the MLAB scheme, a train of radiation pulses with 3 GW power and 1 as FWHM (900 zs in RMS) pulse duration has been obtained at 12.4 keV photon energy. Both schemes generate broadband, discrete, and coherent spectrum compared to the XFEL's narrowband spectrum. Furthermore, the effect of slotted foil is also studied first time on the MLAB-FEL output. Numerical comparisons show that the temporal structure of the MLAB-FEL output can be improved significantly by the use of the slotted foil. Such short X-ray pulses at XFEL facilities will allow the studies of electron-nuclear and nuclear dynamics in atoms or molecules, and the broadband radiation will substantially improve the efficiency of the experimental techniques such as X-ray crystallography and spectroscopy, paving the way for outstanding progress in biology and material science. *Published by AIP Publishing.* [http://dx.doi.org/10.1063/1.4984936]

I. INTRODUCTION

Attosecond science is the area born with the first successful generation of sub-femtosecond extreme ultraviolet (XUV) light via high harmonic generation (HHG) based on femtosecond lasers.[1,2] These sources have paved the way for crucial progress in the understanding of the fundamental processes in matter. For example, time resolved spectroscopy at the femtosecond time scale has opened a new field in femtochemistry for the study of atomic-scale dynamics of chemical bonds.[3] Extending this technique to the attosecond domain would provide an ideal tool for investigating electronic dynamics on the atomic/molecular scale,[4] which is expected to inspire new breakthroughs in ultrafast science.[5,6] These fields will flourish even more with the generation of attosecond/zeptosecond pulses in the X-ray region.

The development of X-ray free electron lasers (XFEL)[7–12] presently surpasses HHG sources[6] in terms of shorter wavelength (by approximately two orders of magnitude) and higher power. Moreover, current XFEL is a superior source to synchrotrons by at least nine orders of magnitude in the intensity, which has set new frontiers in X-ray science. Most XFELs are based on the self-amplified spontaneous emission (SASE) process,[13–15] which has noisy temporal and spectral properties,[16] although using self-seeding scheme allows improving the longitudinal coherence of the SASE XFELs for both the soft and the hard X-ray regimes.[17–20] The current XFEL has its peak power from 10 to 50 GW and its pulse duration of from a few to about 100 femtoseconds at saturation in the X-ray region. High intensity and tunability of the XFEL over a broad spectral range make it a highly versatile light source. This versatility has rendered XFELs highly successful in a wide range of scientific applications.

However, further decrease of the pulse duration of the XFEL is in demand to increase the resolution of X-ray diffraction imaging experiments and to limit the radiation damage on the samples simultaneously. The pulse duration in XFEL is an important parameter. Theoretically, the radiation pulse length can be reduced to a single wavelength. Several schemes in the past were proposed for short pulse generations in XFELs[21–35] using optical lasers and generating short electron bunches.[36–38] Among them, a few methods are surprisingly simple and very attractive particularly because their flexibility makes them applicable at the existing XFEL facilities worldwide. For some cases, low charge electron beam can be used to reduce the electron bunch length as well as the radiation pulse length by about two orders of magnitude.[39] Alternately, one may adopt the emittance spoiler technique which employs a slotted foil in the middle of the bunch compressor to select a small unspoiled part of the electron beam to lase,[38] which is experimentally demonstrated as well.[40]

For terawatt power and attosecond XFEL, Tanaka[32] proposed a scheme that uses the combination of a slotted foil,[36] enhanced SASE (ESASE),[24] and optical and electron beam

[a]Authors to whom correspondence should be addressed: mshur@unist.ac.kr and mchung@unist.ac.kr

delay between undulator sections. Recently, Prat and Reiche[38] proposed a simpler scheme in which a multiple slot foil is used to smear the emittance in some parts of the electron bunch but to preserve the emittance in other parts of the electron bunch. In another work, Kumar *et al.*[34] suggested a new idea where only one single electron spike is used repeatedly. The radiation amplification is based on the superradiant behavior of short pulses,[41,42] where the power level can significantly exceed the saturation power of an XFEL while its pulse length is shortened.

Moreover, decreasing the pulse duration beyond atomic unit of time (24 as) has been examined numerically[26,31] in soft X-ray and hard X-ray FELs, while similar mode-locked (ML) structures have been examined in FEL oscillators in a visible range.[43] In our previous works,[30,33,34] we numerically examined an isolated 100 as full-width half maximum (FWHM) pulse duration with output power varying from gigawatt (GW) to terawatt range at X-ray wavelength. To achieve such short pulses, the electron beam is modulated in energy and density using a 5 fs, 800 nm optical laser before entering to the undulator.

Despite these substantial improvements, further shortening of the radiation pulse would be advantageous as a future upgrade of the XFEL facilities. We present the simulation results of mode locked (ML) FEL[26] scheme and mode locked afterburner (MLAB) FEL[31] scheme based on the PAL-XFEL[12] parameters. The purpose of this paper is to see the feasibility of these schemes in the hard X-ray undulator hall of a typical XFEL facility. Additionally, for first time, we study the effect of slotted foil[36] on the output radiation pattern of the MLAB FEL.[31] In the slotted foil method, a narrow slit width is used to spoil the emittance of most of the e-beam, while leaving a very short unspoiled time-slice that produces the reduced length of the pulse train much shorter than the full electron bunch. The structure of the manuscript is as follows. Section II describes the brief description of both schemes. In Section III, we present the simulation results for hard X-ray beamline using both schemes and the effects of the slotted foil on the MLAB scheme. Finally, in Section IV, conclusions and outlines of future work are presented.

II. SCHEME

Unlike conventional lasers, the FELs' output photon energy can exceed conventional lasers making them a unique and innovative approach for the realization of a tunable, high-intensity, and coherent X-ray source. First, we briefly describe ML-FEL and MLAB-FEL schemes and their working principles in Secs. II A and II B, respectively.

A. Mode-locked FEL scheme

The ML-FEL mainly works on the concept of mode-locked cavity lasers. It generates a set of axial radiation modes similar to the axial cavity modes in the conventional laser oscillators.[44] The ML-FEL has one modulator used to apply an energy modulation to the electron beam. This energy modulated electron beam enters an undulator-chicane setup for radiation amplification. In FEL, the SASE radiation generated in an undulator is relatively noisy and has radiation pulses uncorrelated in phase. To improve the quality of the SASE radiation, the electrons are delayed with respect to the radiation. These electron delays are achieved by repeatedly delaying the electrons via the magnet chicanes added at every inter-undulator section, as shown schematically in Fig. 1(ii). A fixed delay is used for all the added magnet chicanes. This additional electron delay with respect to the radiation in addition to the natural radiation slippage increases the net interaction length of the electron bunch and radiation over that of the simple SASE case, increasing the cooperation length, $l_c = \lambda_r/4\pi\rho$ and the coherence length, $l_{coh} = l_c$ of the interaction, where λ_r is the radiation wavelength and ρ is the FEL parameter. For equal, periodic delays, the radiation spectrum develops discrete frequencies similar to the axial modes of a conventional laser. By introducing an energy modulation at the modulation frequency ω_m, the modes become phase locked to give a temporal train of equally spaced, short, high-power pulses phase-correlated over a distance l_{coh}. This method is known as ML-FEL. In the radiation output, the number of optical cycles per radiation pulse depends on the number of undulator periods chosen in one undulator section of the ML-FEL.

The scheme is shown in Fig. 1: it includes a modulator [Fig. 1(i)] for energy modulation of an electron beam, followed by an undulator-chicane setup [Fig. 1(ii)]. The energy modulation is defined as a sinusoidal variation $\gamma(t) = \gamma_0 + \gamma_m \cos(\omega_m t)$, where γ_0 is the mean energy of the electron beam, γ_m is the modulation energy, and ω_m is the modulation frequency. The regions in which $\gamma \approx \gamma_0 \pm \gamma_m$ are termed as high quality regions due to small energy gradients. Therefore, these regions are supposed to experience a strong FEL interaction within the undulator to generate the comb structure in the electron bunching. In fact, the strong bunching will occur at the minima, $\gamma \approx \gamma_0 - \gamma_m$, of the energy modulation. Other regions will be spoiled due to large energy gradients. As the amplification process starts, the shape of the radiation pulse is replicated in the energy distribution of the electron beam.

B. Mode-locked afterburner scheme

The MLAB-FEL[31] scheme has a slightly modified configuration from the ML-FEL[26] scheme configuration.

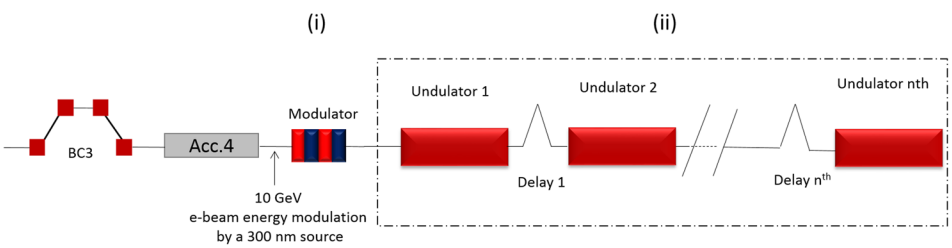

FIG. 1. Schematic layout of mode-locked FEL.[26]

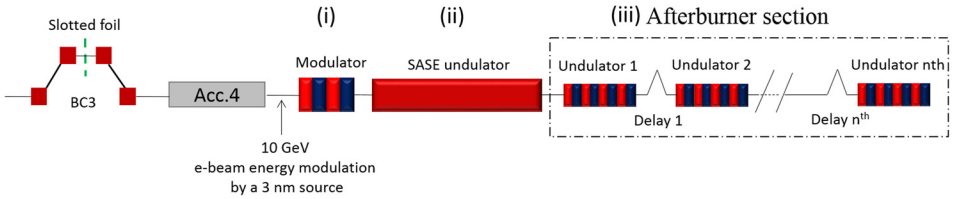

FIG. 2. Schematic layout of mode-locked afterburner scheme.[29]

The schematic layout of the MLAB is shown in Fig. 2: first, a modulator [Fig. 2(i)] is used for an energy modulation of the electron beam followed by a long SASE undulator [Fig. 2(ii)], and then a compact afterburner stage is added after the SASE undulator [Fig. 2(iii)]. The energy modulated electron beam is sent to a long undulator for radiation generation where the pre-energy-modulated beam develops to comb-like radiation spikes due to the FEL-interaction. The length of the SASE undulator is kept shorter than the FEL saturation length. Later, the microbunched beam and radiation are sent together to the afterburner stage, where the small undulator-chicane modules maintain an overlap between the combs of the bunched electrons and the developed radiation. Here, the radiation develops exponentially in power to saturation. Since the amplification occurs over a number of afterburner modules, the pulses are delivered in trains and can be naturally synchronized to the modulating laser.

III. RESULTS AND DISCUSSION

The PAL-XFEL[12] is a 0.1 nm, SASE-based high power, short pulse X-ray coherent photon source. It provides 10^{12} photon/pulse using a 0.2 nC/10 GeV ($\gamma = 2 \times 10^4$) electron S-band normal conducting Linac. The photon flux of 10^{12} at 0.1 nm corresponds to 30 GW radiation power with the pulse length of 60 fs in FWHM. In the self-seeding mode of the PAL-XFEL,[45] the radiation-bandwidth below 5×10^{-5} can be achieved for hard X-ray FEL. The radiation produced by 10 GeV electron beam in the undulator has been computed by a three-dimensional time-dependent FEL code GENESIS.[46] Figure 3(a) shows the oscillation pattern of the SASE radiation power at 60 meter of the undulator. Figure 3(b) shows the corresponding typical FEL power spectra with narrow bandwidth. Full description of the electron beam and undulator parameters of the 10 GeV PAL-XFEL is shown in Table I.

A. Mode-locked FEL simulation study with PAL-XFEL

First, we study the attosecond pulse generation using the ML-FEL[26] scheme with the PAL-XFEL[12] parameters. We focus on the hard X-rays with photon energy of 12.4 keV. The electron beam is modulated in energy by a 30 nm source with a long scale period relative to the FEL resonant wavelength, $\lambda_r \sim 0.1$ nm. We choose an optimized energy modulation amplitude of 0.06% before entering the undulator. This energy modulated electron beam is injected to the undulator-chicane stages of the ML-FEL. The undulator module is relatively short (72 λ_u), compared to the standard PAL-XFEL undulator module (190 λ_u), where λ_u is 2.6 cm. During electron beam and radiation interaction, the radiation slips ahead by λ_r in one undulator period λ_u. Total radiation slippage inside one undulator section is $l \sim 72\ \lambda_r$. A fixed delay $\delta \sim 228\ \lambda_r$ is applied to the electron beam by the magnet-chicane present in-between two undulator modules. The net delay of one undulator-chicane stage is $s \sim (72\ \lambda_r + 228\ \lambda_r)$, where λ_r is the radiation wavelength. The slippage enhancement factor is $S_l = (s/l) \sim 5$. A magnet-chicane is a set of four-dipole-magnets which is controlled by momentum compaction factor $R_{56} = -2\theta_B^2(L_1 + 2/3L_B)$, where θ_B is the bending angle of the electron trajectory inside the chicane, L_1 is the length between the first and the second (and also third and fourth dipole magnets), and 2 L_B is the magnet length. Approximating $R_{56} \simeq 10\delta/3$,[26] the required electron beam delay δ can be applied by controlling the bending angle θ_B and L_1 parameters of the magnet-chicane.

Figure 4(a) shows the output power profile after 18 undulator-chicane stages of the ML-FEL. The power profile shows a series of several radiation spikes, where each radiation spike is ~16 as in FWHM and separated by ~54 as with each other. Maximum power after 18 undulator-chicane stages is 3.5 GW. Figure 4(b) shows the ML-FEL spectra which consist of broadband, discrete bandwidth spectrum.

Because the ML-FEL uses shorter undulator module (72 λ_u) than the standard undulator module of the PAL-XFEL

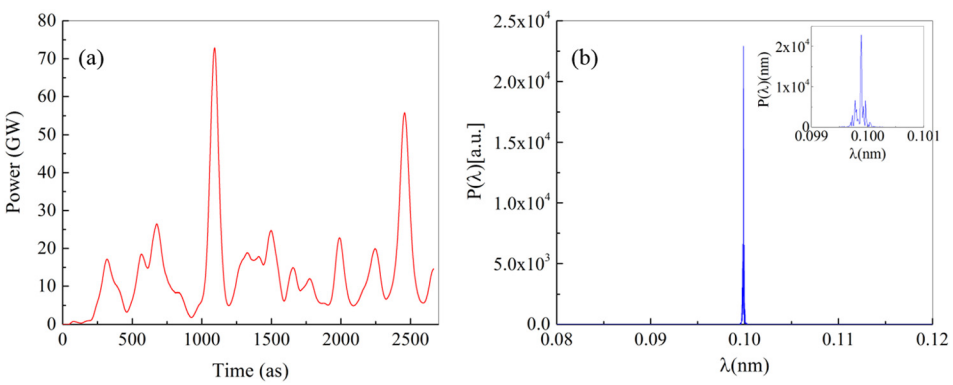

FIG. 3. (a) Plot of the temporal profile of the SASE output power after 60 m long undulator (no initial beam-energy modulation) and (b) typical SASE power spectra (inset is enlarged plot showing noisy spectral structure).

TABLE I. PAL-XFEL related parameters.

Electron beam parameters (units)	Values
Electron beam energy E (GeV)	10
Beam current I (kA)	3000
Normalized emittance ε_n (mm-mrad)	0.2
RMS fractional energy spread σ_γ/σ_0	1×10^{-4}
Undulator period λ_u (cm)	2.6
Standard Undulator module (units l/λ_u)	190
Resonance wavelength λ_r (nm)	0.1
FEL parameter ρ	7×10^{-4}

(190 λ_u), this scheme requires major modification of the existing FEL beamline. However, the MLAB scheme is potentially a simple upgrade to the existing X-ray FEL facilities. We discuss the simulation results of the MLAB scheme in Sec. III B.

B. Mode-locked after-burner scheme results with PAL-XFEL

In the MLAB simulation, at first, the electron beam is energy modulated by a relatively short length scale source, i.e., a 3 nm source. Such a source is easily available using HHG lasers.[47] The energy modulation amplitude is determined to be $\gamma_m/\gamma_0 \approx \rho$. The energy modulated electron beam is injected to a long SASE undulator for radiation amplification. The SASE undulator consists of six 190-period undulator modules with its period length ~2.6 cm. We choose the first 35-m-long undulator for normal SASE amplification.

Figure 5(a) shows the growth of the radiation power along a 60 m long undulator, and Fig. 5(b) shows the longitudinal profiles of the radiation power generated in a 35 m long SASE undulator for a range of energy modulations of the beam. One can see small undulation of the radiation power on the scale λ_m. For afterburner simulation, $\gamma_m/\gamma_0 = 0.06\%$ energy modulation is chosen. After the SASE amplification stage, the modulated electron beam and radiation are fed into the afterburner stage. Each afterburner module has eight undulator periods followed by a magnet-chicane that delays the electron beam by 22 resonant wavelengths. The net delay per undulator-chicane module is $s \sim (l+\delta)/l = 30\lambda_r = \lambda_m$, where $l \sim 8\lambda_r$ is the radiation slippage and $\delta \sim 22\lambda_r$ is the electron beam delay. Using a fixed electron beam delay via small chicanes, the bunching comb and radiation comb are overlapped and rephased regularly in the afterburner stage. As a result, the radiation pulse structure develops rapidly and the radiation amplification grows exponentially compared to the normal SASE amplification inside the amplifier stage. The radiation amplification also depends on the magnet chicanes as they provide the additional bunching[26] to the electron beam. The temporal pulse train structure of the radiation profile develops further as we add more and more undulator-chicane stages in the afterburner.

Figure 5(c) shows the temporal profile of the radiation power at the exit of the afterburner stage. After 40 undulator/chicane modules in the afterburner, the output consists of a train of 1.33 as FWHM (~900 zs RMS) radiation pulses. The separation of the radiation pulse is 10 as, which is similar to the modulation wavelength ~3 nm (~412 eV in photon energy). The lengths of each undulator module and the magnet-chicane module are 0.20 m and 0.26 m, respectively. Figure 5(d) shows the power spectrum which is multichromatic with the bandwidth envelope increased by a factor ~100 over normal SASE-FEL spectrum. However, more simulations and optimizations of these undulator and chicane structures are necessary to fully understand the functioning of the small undulator and magnet chicane of the afterburner stage.

C. Using slotted foil along with mode-locked afterburner

To improve the radiation profile of Fig. 5(c), we use the emittance spoiler method.[36] According to this method, a slotted foil is inserted in the central part of the third bunch compressor (BC3) of the PAL-XFEL linac, as shown in Fig. 2. The slotted foil mainly deteriorates the emittance properties of the head and tail parts of the longitudinal distribution of the electron beam, and a small unspoiled section of the electron beam is chosen to lase inside the undulator. The head and tail parts of the electron bunch have their emittances increased several times. Therefore, the larger emittance of the spoiled beam suppresses the FEL amplification at the head and tail parts of the electron bunch. The unspoiled, a very short slice of the bunch however experiences FEL gain and will reach full power saturation. The method offers simplicity and flexibility and can be added to an existing FEL without significant cost or design alterations. The slotted foil may contain single or multiple slots with varying spacing.[38] Only the electron-bunch slices

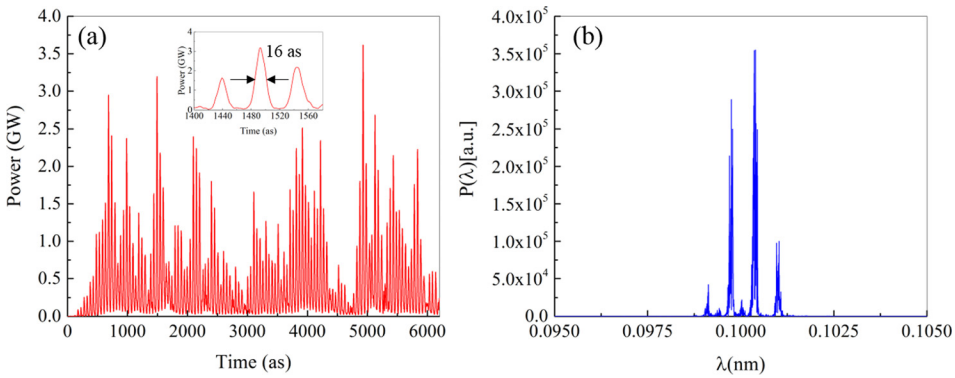

FIG. 4. ML-FEL simulation result with PAL-XFEL hard X-ray beamline. (a) Shows the attosecond pulse train of hard X-rays at 12.4 keV photon energy after 18 undulator-chicane modules. (b) Shows the ML-FEL spectrum. The corresponding spectrum is broadband and discretely multichromatic.

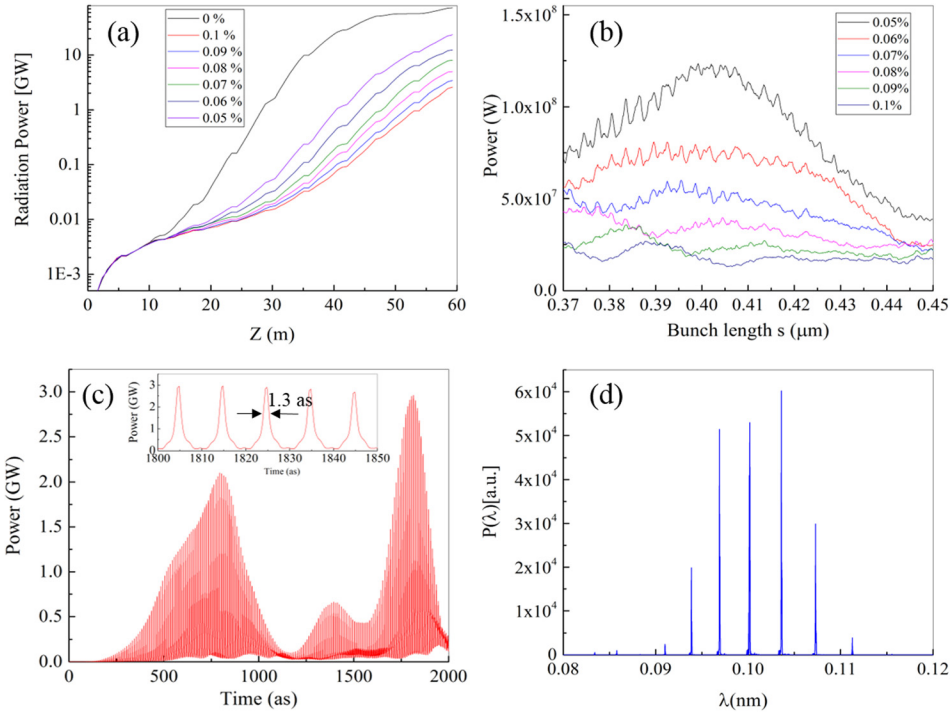

FIG. 5. (a) Shows the radiation power along the undulator length for different electron-beam energy modulations at the entrance of the undulator, (b) shows the longitudinal profiles of radiation power taken at the end of 35 m long SASE undulator for different energy modulations of the electron beam, (c) shows the attosecond pulse train of hard X-rays at 12.4 keV photon energy after 40 undulator-chicane modules using MLAB scheme (inset plot shows the enlarge view of a train of attosecond pulses), and (d) shows the corresponding power spectrum.

passing through the slot will have the small emittance required to produce XFEL radiation.

Figure 6(a) shows the normalized electron-beam emittance $\epsilon_{x,y}$ at the undulator entrance. The black-dotted line represents the normalized emittance without the slotted foil, while the red-line represents the emittance in the presence of the slotted foil. Only low emittance slot in the red-line plot will contribute to producing efficient XFEL radiation along the SASE undulator. Figure 6(b) shows the radiation power at the end of 35 m long SASE undulator. Without the slotted foil (black-line), the temporal profile of the radiation power consists of several radiation spikes and the maximum power is ∼0.08 GW. However, with the slotted foil (red-line), a single radiation spike is generated with a reduced power ∼0.04 GW. The reduction in power is quite obvious, as the use of the slotted foil limits significantly the number of electrons contributing to the lasing process. Now, the slotted electron-beam and the radiation pulse pass through the afterburner stage together for further exponential amplification of the radiation. Figure 7 shows the radiation profile after 40 undulator-chicane modules of the afterburner stage. Using the slotted foil, the net power gain (∼0.4 GW) is reduced compared to the case without the slotted foil [∼2.5 GW in Fig. 5(c)]. After adding more undulator-chicane modules to the afterburner stage, the radiation power can be increased further.

If we look at Fig. 5(c), the temporal radiation output of the original ML-AB scheme, the train of very short pulses is modulated by SASE envelope, and within each lobe of this envelope the radiation spikes have the same phases and hence they are temporally coherent but from one lobe to another the phase is different. Therefore, different phases in different lobes may limit the applicability of this scheme for XFEL users. However, using slotted foil, the ML-AB output can be reduced to a pulse train with an envelope having a single lobe and the phase of each spike will be constant along the output pulse, which may offer benefits to the users. Inset (a) of Fig. 7 shows the corresponding power spectrum which is almost 100 times larger than the typical SASE spectrum. Inset (b) of Fig. 7 shows few radiation pulses, where each one has ∼1.3 as pulse duration with mutual separation of 10 as.

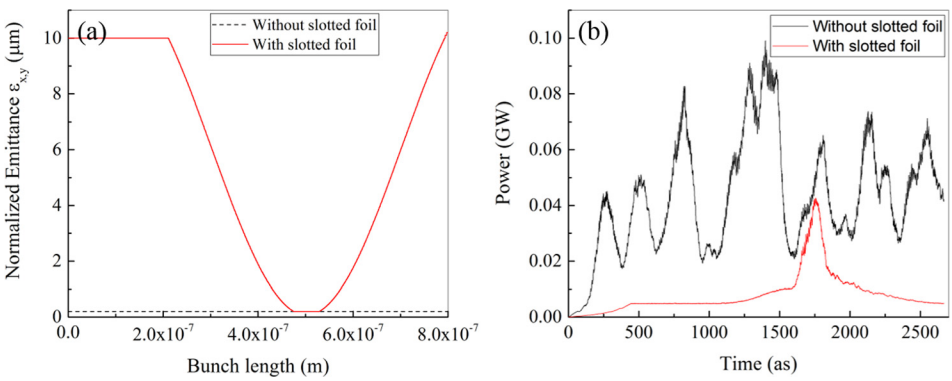

FIG. 6. (a) Normalized horizontal and vertical emittances ($\epsilon_{x,y}$) along the longitudinal position of the electron bunch and (b) the temporal profiles of the radiation power at 35 m of the SASE undulator in MLAB with and without slotted foil.

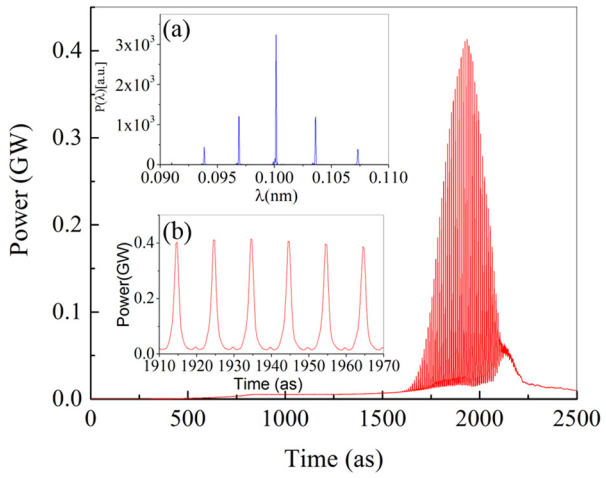

FIG. 7. Plot of an attosecond pulse train of hard X-ray at 12.4 keV photon energy after 40 undulator-chicane modules amplification in MLAB scheme with slotted foil. Inset (a) shows the corresponding power spectra and inset (b) shows the enlarged view of attosecond pulse train. Here, 0.06% electron beam energy modulation is considered before entering to the undulator.

IV. CONCLUSIONS

Numerical simulations are performed for the hard X-ray beamline of 10 GeV PAL-XFEL to assess the performance of the ML-FEL and MLAB-FEL schemes.[26,31] Both schemes are intended to minimize the radiation pulse duration in XFEL. Our simulation results indicate that a pulse train of 16 as pulse radiation (54 as mutual separation) with 3.5 GW power is achieved using 18 undulator-chicane modules (∼42 m long) in the ML-FEL scheme at 12.4-keV photon energy. On the other hand, using the MLAB-FEL, a pulse train of radiation with 3 GW power and 1.3 as pulse duration is achieved at 12.4-keV photon energy in a ∼43 m long afterburner undulator system. To further improve the temporal radiation profile of the MLAB scheme, we use the slotted foil in the bunch-compressor section to spoil the emittances of the head and tail parts of the beam. It is observed that the ML-AB output can be reduced to a pulse train with an envelope having a single lobe and the phase of each spike is constant all the way along the output pulse which may be useful for X-ray crystallography experiments.

In conclusion, both schemes are analyzed with the PAL-XFEL parameters. The schemes are simple, attractive and flexible, which makes them applicable over a wide range of FEL parameters. The ML scheme requires substantial change in the PAL-XFEL undulator structure. However, the realization of the ML-afterburner scheme is promising with the existing PAL-XFEL undulator. Therefore, the MLAB scheme is more favorable for its simplicity and ease of implementation and allows a very compact undulator beamline. Additional work on afterburner optimization is in progress for the pulse shaping in the attosecond domain, which may further increase the attractiveness of the MLAB-FELs, as it makes possible new kinds of experiments that require very short and high-power FEL pulses.

ACKNOWLEDGMENTS

This work was supported by the National Research Foundation of Korea (NRF) Grant funded by the Korean Government (MSIP) (No. 2016R1A5A1013277). We would like to thank Dr. Neil Thompson and Dr. David Dunning from the STFC, Daresbury Laboratory, U.K., for the fruitful discussions about ML and MLAB-FEL schemes.

[1]P. M. Paul, E. S. Toma, P. Breger *et al.*, Science **292**, 1689–1692 (2001).
[2]M. Hentschel, R. Kienberger, C. Spielmann *et al.*, Nature **414**, 509–513 (2001).
[3]A. H. Zewail, J. Phys. Chem. A **104**, 5660 (2000).
[4]Z. Chang and P. Corkum, J. Opt. Soc. Am. B **27**, B9 (2010).
[5]P. H. Bucksbaum, Science **317**, 766 (2007).
[6]F. Krausz and M. Ivanov, Rev. Mod. Phys. **81**, 163 (2009).
[7]W. A. Ackermann *et al.*, Nat. Photonics **1**, 336 (2007).
[8]P. Emma *et al.*, Nat. Photonics **4**, 641 (2010).
[9]T. Ishikawa *et al.*, Nat. Photonics **6**, 540 (2012).
[10]E. Allaria *et al.*, Nat. Photonics **7**, 913 (2013).
[11]C. Pellegrini, A. Marinelli, and S. Reiche, Rev. Mod. Phys. **88**, 015006 (2016).
[12]H. S. Kang, H. H. Han, C. Kim *et al.*, in *Proceedings of IPAC 2013, Shanghai, China* (2013), p. 2074.
[13]A. M. Kondratenko and E. L. Saldin, Part. Accel. **10**, 207 (1989).
[14]R. Bonifacio, C. Pellegrini, and L. M. Narducci, Opt. Commun. **50**, 373 (1984).
[15]G. Dattoli, A. Marino, A. Renieri, and F. Romanelli, IEEE J. Quantum Electron. **17**, 1371 (1981).
[16]H. Hauss, IEEE J. Quantum Electron. **17**, 1427 (1981).
[17]J. Feldhaus, E. L. Saldin, J. R. Schneider *et al.*, Opt. Commun. **140**, 341 (1997).
[18]E. L. Saldin, E. A. Schneidmiller, Y. V. Shvyd'ko *et al.*, Nucl. Instrum. Methods Phys. Res., Sect. A **475**, 357 (2001).
[19]G. Geloni, V. Kocharyan, and E. Saldin, DESY Report No. 10-053, 2010.
[20]J. Amann *et al.*, Nat. Photonics **6**, 693–698 (2012).
[21]E. L. Saldin, E. A. Schneidmiller, and M. V. Yurkov, Opt. Commun. **239**, 161–172 (2004).
[22]A. A. Zholents and W. M. Fawley, Phys. Rev. Lett. **92**, 224801 (2004).
[23]E. L. Saldin, E. A. Schneidmiller, and M. V. Yurkov, Phys. Rev. ST Accel. Beams **9**, 050702 (2006).
[24]A. A. Zholents, Phys. Rev. ST Accel. Beams **8**, 040701 (2005).
[25]A. A. Zholents and M. S. Zolotorev, New J. Phys. **10**, 025005 (2008).
[26]N. R. Thompson and B. W. J. McNeil, Phys. Rev. Lett. **100**, 203901 (2008).
[27]D. Xiang, Z. Huang, and G. Stupakov, Phys. Rev. ST Accel. Beams **12**, 060701 (2009).
[28]Y. Ding, Z. Huang, D. Ratner *et al.*, Phys. Rev. ST Accel. Beams **12**, 060703 (2009).
[29]S. Y. Chung, M. Yoon, and D. E. Kim, Opt. Express **17**, 7853–7861 (2009).
[30]S. Kumar, H. S. Kang, and D. E. Kim, Opt. Express **19**, 7537 (2011).
[31]D. J. Dunning, B. W. J. McNeil, and N. R. Thompson, Phys. Rev. Lett. **110**, 104801 (2013).
[32]T. Tanaka, Phys. Rev. Lett. **110**, 084801 (2013).
[33]S. Kumar, H. S. Kang, and D. E. Kim, Opt. Express **23**, 2808 (2015).
[34]S. Kumar, Y. W. Parc, A. S. Landsman, and D. E. Kim, Sci. Rep. **6**, 37700 (2016).
[35]S. Huang, Y. Ding, Z. Huang, and G. Marcus, Phys. Rev. ST Accel. Beams **19**, 080702 (2016).
[36]P. Emma, K. Bane, M. Cornacchia *et al.*, Phys. Rev. Lett. **92**, 074801 (2004).
[37]S. Reiche, P. Musumeci, C. Pellegrini *et al.*, Nucl. Instrum. Methods Phys. Res., Sect. A **593**, 45 (2008).
[38]E. Prat and S. Reiche, Phys. Rev. Lett. **114**, 244801 (2015).
[39]Y. Ding *et al.*, Phys. Rev. Lett. **102**, 254801 (2009).
[40]Y. Ding *et al.*, Phys. Rev. Lett. **109**, 254802 (2012).
[41]R. Bonifacio, L. D. S. Souza, P. Pierini *et al.*, Nucl. Instrum. Methods Phys. Res., Sect. A **296**, 358–367 (1990).
[42]R. Bonifacio, N. Piovella, and B. W. J. McNeil, Phys. Rev. A **44**, R3441 (1991).
[43]P. L. Ottaviani, S. Pagnutti, G. Dattoli *et al.*, Nucl. Instrum. Methods Phys. Res., Sect. A **834**, 108 (2016).
[44]A. E. Siegman, *Lasers* (University Science Books, Sausalito, USA, 1986), Chap. 27.
[45]J. Lee, C. H. Shim, M. Yoon *et al.*, Nucl. Instrum. Methods Phys. Res., Sect. A **798**, 162–166 (2015).
[46]S. Reiche, Nucl. Instrum. Methods Phys. Res., Sect. A **429**, 243–248 (1999).
[47]T. Popmintchev *et al.*, Science **336**, 1287 (2012).